IEEE Photonics Journal
An IEEE Photonics Society Publication

Theoretical and Experimental Optimum System Design for LTE-RoF Over Varying Transmission Span and Identification of System Nonlinear Limit

Volume 4, Number 5, October 2012

W. P. Ng, Senior Member, IEEE
T. Kanesan, Student Member, IEEE
Z. Ghassemlooy, Senior Member, IEEE
C. Lu, Member, IEEE

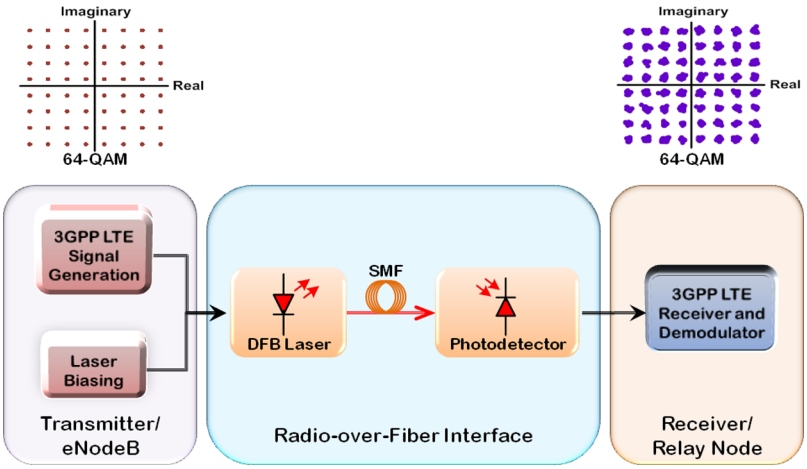

DOI: 10.1109/JPHOT.2012.2211343
1943-0655/$31.00 ©2012 IEEE

Theoretical and Experimental Optimum System Design for LTE-RoF Over Varying Transmission Span and Identification of System Nonlinear Limit

W. P. Ng,[1] *Senior Member, IEEE*, T. Kanesan,[1] *Student Member, IEEE*, Z. Ghassemlooy,[1] *Senior Member, IEEE*, and Chao Lu,[2] *Member, IEEE*

[1]Optical Communications Research Group, NCR Laboratory, School of Computing, Engineering and Information Sciences, Northumbria University, NE1 8ST Newcastle Upon Tyne, U.K.
[2]Photonics Research Center, Department of Electronics and Information Engineering, The Hong Kong Polytechnic University, Kowloon, Hong Kong

DOI: 10.1109/JPHOT.2012.2211343
1943-0655/$31.00 ©2012 IEEE

Manuscript received June 30, 2012; revised July 24, 2012; accepted July 26, 2012. Date of publication August 14, 2012; date of current version August 17, 2012. Corresponding authors: W. P. Ng (e-mail: wai-pang.ng@northumbria.ac.uk; thavamaran.kanesan@northumbria.ac.uk; z.ghassemlooy@northumbria.ac.uk; Chao.Lu@inet.polyu.edu.hk).

Abstract: This paper proposes an optimum radio-over-fiber (RoF) system design to extend the coverage of the third-generation partnership program (3GPP) long-term evolution (LTE) base station, i.e., eNodeB. The system is theoretically and experimentally demonstrated as the high-speed interface between eNodeB and a relay node. The LTE signals under test comprise three different modulation schemes, namely, quaternary phase-shift keying (QPSK), 16-quadratic-amplitude modulation (QAM), and 64-QAM, which are modulated onto orthogonal frequency-division multiplexing (OFDM) at 2.6 GHz. The RoF system design is based on the distributed feedback (DFB) laser direct modulation and direct detection receiver. The spurious-free dynamic range (SFDR) considering the third-order intermodulation analysis of the DFB laser achieved 1.93-dB dynamic range gain to improve the modulation efficiency. The practical investigation reveals three distinctive optical power transmission regions, namely, linear, intermixing, and nonlinear regions. The QPSK, 16-QAM, and 64-QAM systems in the intermixing region achieved error vector magnitudes (EVMs) of ∼1.144%, ∼1.2%, and ∼1.21%, respectively, for 10-km transmission, whereas at 60 km, the achieved EVMs are ∼5.86%, ∼5.96%, and ∼6.01%, respectively. The intermixing region for the 10–60-km transmission span achieved the most optimized EVM and within the 3GPP LTE limit of 8%. Additionally, we also demonstrate that nonlinear distortion proportionally increases with linear distortion as the transmission span increases.

Index Terms: Long-term evolution (LTE), optical orthogonal frequency-division multiplexing (OOFDM), radio-over-fiber (RoF).

1. Introduction

The third-generation partnership program (3GPP) long-term evolution (LTE) group is working on the mobile broadband access to meet the coverage and throughput according to the fourth-generation requirements [1]. Precisely, it is an evolution to the existing 3GPP radio technologies and a development path for the Global System for Mobile Communications and Universal Mobile Telecommunication Systems [2]. The main challenge in meeting this requirement is to maintain a consistent throughput at cell edges of an eNodeB (eNB), which is the LTE base station. In this context, the

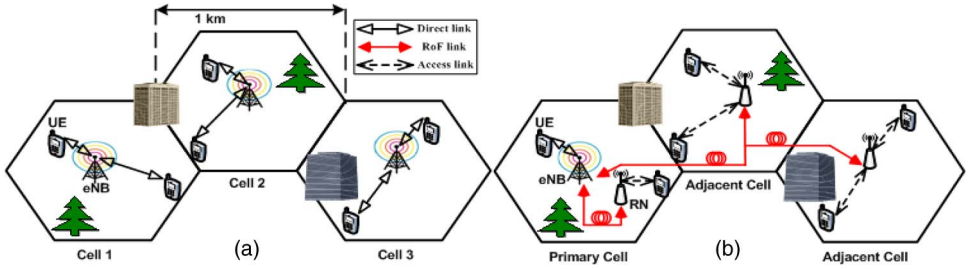

Fig. 1. Full duplex LTE radio access network structure for (a) without RN and (b) with RN in urban area.

LTE physical layer consists of complex technologies including orthogonal frequency-division multiplexing (OFDM) with various types of single-carrier modulation (SCM). However, complex technologies would not improve the throughput at the cell edge because the LTE broadband radio interface is characterized by its limited transmission range due to high operating carrier frequencies [3]. For example, a 25-Mb/s LTE signal transmitted at the 2.6-GHz band in the urban area of Europe has a cell radius of 1 km [4]. As a result, LTE network deployment would require high density of eNB in order to achieve the acceptable capacity, radio coverage, and quality of service (QoS). Since eNB is complex in design employing advance signal processing and smart antenna technique [5], therefore deployment of eNB would cause a striking rise in the total cost of ownership, hence higher cost per delivered bit.

Real-time data from [1] show that the user equipment (UE) potentially receives a data rate of less than 20 Mb/s at the cell edge from eNB with a non-line-of-sight (NLOS) path in an urban environment. One reliable solution to improve the cell-edge performance is to employ a fixed relay node (RN) using radio relaying. The current LTE structure would be more efficient in terms of the capacity, coverage, QoS, and deployment cost with using RN as a key structure to extend the cell coverage, instead of deploying additional eNB. In the previous reported work, RN with the decode-and-forward scheme has been proposed, where the achieved coverage extension reported was only 3.2 km with the radio frequency (RF) wireless line-of-sight connectivity between eNB and RN [1], [4]. Nagate *et al.* [6] extended the eNB cell size up to 2.1 km with a multicooperative scheme and radio-over-fiber (RoF) as the interface. In addition, commercial LTE-RoF integration has been realized for the indoor distributed antenna system by Zinwave to overcome RF signal penetration losses for in-building applications [7], while we theoretically demonstrated the outdoor eNB cell extension of up to 68 km with the amplifying-and-forwarding (AF)-based RN [8]. The deployment cost of optical fiber for the outdoor eNB coverage extension can be reduced by reusing the existing legacy fiber backhaul infrastructures in the urban area [9]. For the rest of the paper, RN only refers to the AF scheme with the signal amplification and retransmission and no further processing. Fig. 1(a) shows the existing field deployment by 3GPP, where eNB is deployed at every consecutive cell with a 1-km radius. Cells are labeled as cell 1, cell 2, and cell 3; the eNB is directly connected to the UE within the respective cell. In Fig. 1(b), our proposed method is to connect eNB and UE at the cell edge via RN within the primary cell by employing the RoF interface. As a result, single-eNB coverage is extended to the adjacent cell at the same carrier frequency of 2.6 GHz with the RoF interface. The rationale for such strategy is to reduce the deployment cost of LTE in an urban area.

For the first time, this paper presents a comprehensive theoretical and experimental analysis of the full system with a directly modulated LTE-RoF link.

The modulation analysis is carried out by applying two-tone intermodulation (IMD). The nonlinear response of the distributed feedback (DFB) laser in a back-to-back system could be verified with a two-tone IMD, which provides the spurious-free dynamic range (SFDR). There are also RoF links based on an external modulation [8], [10]. Technically, the external modulation provides negligible positive frequency chirp (PFC), which could achieve a longer transmission span and makes it superior to the direct modulation. However, the shortcoming of external modulation is the higher cost of requiring an external modulator. Since [8] has theoretically shown that the direct-modulation-based

link for LTE-Advanced could provide a transmission span of up to 68 km, this paper will focus on the experimental direct modulation for a maximum transmission span up to 60 km due to the availability of single-mode fiber (SMF) in our laboratory.

In terms of propagation analysis, we are transmitting the direct detection (DD) optical OFDM (OOFDM) signal over three distinctive optical power transmission regions, namely, linear, intermixing, and nonlinear regions. We have used fiber spans of 10, 25, 35, 50, and 60 km. The linear region experiences joint distortion from PFC and chromatic dispersion (CD). The intermixing region provides the optimized optical launch power (OLP) by an interchangeable compensation between PFC and CD with the optical fiber nonlinearity without any additional components. The interchangeable compensation within the intermixing region is viable because PFC- and CD-induced distortion exhibits blue and red rising and trailing edges, respectively; in other words, the signal would spread as it propagates down the fiber. Conversely, the nonlinear induced distortions experience red and blue rising and trailing edges, respectively; hence, the signal would face a compression effect as it propagates. The mixing of these elements would produce a reduced distortion region, which is the intermixing region in this case. Since the SMF used is dispersive at the C-band wavelengths, four-wave mixing effect is considered to be negligible [11]. Owing to the single-wavelength transmission, the cross-phase modulation is omitted in the real-time propagation [11]. Thus, the effects in the nonlinear region are constrained to the self-phase modulation (SPM) and stimulated Brillouin scattering (SBS). Ramos *et al.* [12] initially proposed the intermixing-region-based compensation with no dispersion compensation fiber, and the work was limited to the frequency-length product analysis for a simple binary transmission system. Bao and Shieh [13] showed that the optimized OLP for each channel in coherent optical-OFDM (CO-OFDM) systems are within the range of -10 dBm to -8 dBm. In [14]–[16], the effect of nonlinearity-induced power penalty for the DD-OOFDM link was demonstrated. However, in these investigations, the linear and intermixing regions were not considered. Kanesan *et al.* [8] theoretically analyzed the linear, intermixing, and nonlinear region for LTE-RoF in a fixed transmission range, which form the basis of the proposed system in this paper.

Jarajreh *et al.* [17], [18] carried out full optimization for CO-OFDM, but this optimization cannot be used as a guideline for DD-OOFDM in LTE-RoF system design. This is due to the fact that we aim to design the LTE-RoF link with the DD method, which is widely adopted in commercial designs compared with complex coherent detection systems. Technically, in coherent detection schemes, the optical carrier signal is dropped prior to the detection. In contrast, DD converts optical sidebands with the optical carrier into the respective electrical signal. Therefore, PFC and CD with SPM and SBS induced phase distortions will result in loss of phase coherence in the optical carrier and optical double sideband. Such distortion will be directly converted into the intensity noise by DD due to the nature of signal beating [19]. The intensity noise is less dominant if the correct optical power transmission region is chosen, as the paper will show in later sections.

The paper is organized as follows. Section 2 presents the two-tone IMD analysis. In Section 3, the description of the analytical model of the system, OLP analysis, and linear and nonlinear threshold are shown. Finally, Section 4 concludes the findings of the paper.

2. Two-Tone IMD Analysis

In order to maintain a low-cost system, the proposed RoF link is designed with intensity modulation (IM) by directly modulating a DFB laser. The direct modulation exhibits nonlinear characteristics due to the gain compression, which results from several factors, namely, gain saturation, spatial hole burning, and leakage current [20]. The nonlinear response will result in spurious signals, which are also known as harmonics and IMDs. Harmonics is independent of the input signal, which means harmonics will occur even with the single-tone input. In contrast, IMDs only occur for input signals with more than one tone. Furthermore, harmonics are spurious signals that occur at a distance from the fundamental frequency, and the even-order IMDs have similar response. A two-tone IMD analysis is sufficient to characterize the spurious signals, for both harmonics and IMDs [21]. The output of the DFB laser with respect to the light–current curve can be described with Taylor series

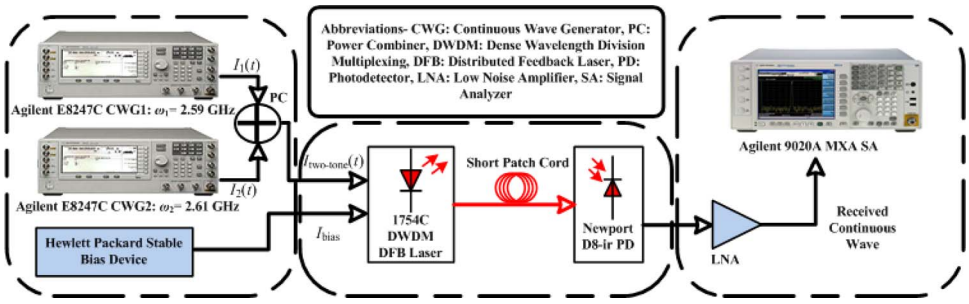

Fig. 2. Experimental setup of two-tone signal for IMD analysis.

$$L(I(t)) = a_1 I(t) + a_2 I^2(t) + a_3 I^3(t) + \ldots \tag{1}$$

where $L(I(t))$ is the output optical power that operates as a function of input current $I(t)$, and a_n represents the coefficient of polynomial fitting on the curve with respect to the order n. $I(t)$, $I^2(t)$, and $I^3(t)$ are the fundamental, second-order spurious, and third-order spurious signals, respectively. The two-tone input can be expressed as

$$I_{\text{two-tone}}(t) = I_1(t) + I_2(t) = A(\cos(\omega_1 t) + \cos(\omega_2 t)) \tag{2}$$

where $I_{\text{two-tone}}(t)$ is the composite signal of the first tone $I_1(t)$ modulated at a frequency ω_1 and the second tone $I_2(t)$ modulated at a frequency ω_2, and A is the magnitude of the applied current. The first tone $I_1(t)$ and second tone $I_2(t)$ are transmitted at frequencies ω_1 of 2.59 GHz and ω_2 of 2.61 GHz. The spacing between ω_1 and ω_2 is 20 MHz, which represents the bandwidth of the LTE signal.

The second-order spurious signals can be expressed as

$$\begin{aligned} a_2 I(t)^2 &= a_2(A\cos(\omega_1 t) + A\cos(\omega_2 t))^2 \\ &= a_2\left\{\frac{A^2}{2}(1+\cos(2\omega_1 t)) + \frac{A^2}{2}(1+\cos(2\omega_2 t)) + A^2(\cos(\omega_1-\omega_2)t + \cos(\omega_1+\omega_2)t)\right\} \end{aligned} \tag{3}$$

where the first and second terms of the solution of (3) comprise second-order harmonics at the frequency multiples of ω_1 and ω_2. The third and fourth terms show the second-order IMD products. The second-order harmonics and IMDs are outside the band, and therefore, they will be omitted for the rest of the analysis. However, the odd-order IMDs tend to be close to the transmitting signal. Therefore, only the third-order IMD is considered in this analysis, as that is the only component that falls closely to the fundamental signal [22]. The analytical expression focusing on the third-order IMD can be shown as:

$$\begin{aligned} A_2 I^3 &= a_3(A\cos(\omega_1 t) + A\cos(\omega_2 t))^3 \\ &= a_3\left\{A^3\left(\cos^3(\omega_1 t)\right) + A^3\left(\cos^3(\omega_2 t)\right) + 3A^3\left(\cos^2(\omega_1 t)\cos(\omega_2 t)\right) + 3A^3\left(\cos^2(\omega_2 t)\cos(\omega_1 t)\right)t\right\} \\ &= a_3\left\{\frac{A^3}{4}\cos(3\omega_1 t) + \frac{A^3}{4}\cos(3\omega_2 t) + \frac{1}{2}\cos(2\omega_1 t - \omega_2 t)\right. \\ &\quad \left. + \frac{1}{2}\cos(2\omega_1 t + \omega_2 t)) + \frac{1}{2}\cos(2\omega_2 t - \omega_1 t) + \frac{1}{2}\cos(2\omega_2 t + \omega_1 t))\right\}. \end{aligned} \tag{4}$$

In (4), the solution shows the first and the second terms, which are the third-order harmonics, and these terms are clearly outside the band and could easily be filtered. The fourth and sixth terms of (4) tend to be outside the band as well. Finally, the most critical terms that are closer to the fundamental frequency are the third and fifth terms of (4), where frequencies are 2.57 and 2.63 GHz, respectively.

In order to characterize SFDR with respect to the third-order IMDs, the two-tone IMD signal analysis is carried out theoretically and experimentally. Fig. 2 shows the experimental setup for the

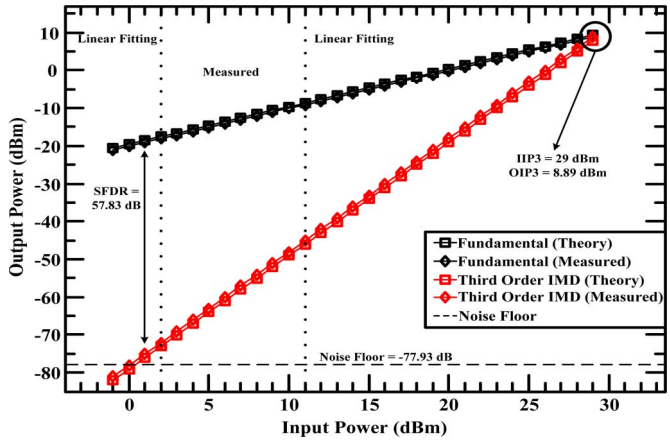

Fig. 3. First- and third-order output powers with respect to input power.

two-tone signal transmission for IMD analysis. Two Agilent E8247C continuous-wave generators (CWGs), CWG1 and CWG2, were utilized to generate signals at ω_1 of 2.59 GHz and ω_2 of 2.61 GHz, respectively. The generated signals are composed of sinusoidal signals; these signals are then summed to form a two-tone signal. The two-tone signal is then directly applied to the 1754C dense wavelength-division-multiplexing-type DFB laser to perform IM. The DFB laser bias current I_{bias} is 60 mA. The optical two-tone signal is then transmitted over a short patch cord and detected via Newport D8-ir photodetector (PD) employing DD. The signal is subsequently amplified to mitigate the conversion loss induced by PD, and SFDR measurement is carried out using an Agilent 9020A MXA signal analyzer (SA).

Fig. 3 depicts theoretical and experimental outcomes of the two-tone IMD analysis. The input powers of $I_1(t)$ and $I_2(t)$ are investigated in the range of 2–11 dBm via CWG1 and CWG2, respectively, after taking the 5-dB loss of the power combiner into consideration. When the input power is below 2 dBm, it is difficult to observe the third-order IMD as it is very close to the noise floor of -77.93 dB. Meanwhile, since the limit of CWG is 16 dBm (which effectively means an input power of 11 dBm due to the power combiner's loss), the linear prediction technique is used to estimate the output power for the given input power below 2 dBm and above 11 dBm. All factors have similar consideration between theory and experiment to maintain the consistency; additionally, it is important to state that all the output metrics presented in Fig. 3 are integrated over a 20-MHz bandwidth. The third-order input/output intercept point (IIP3/OIP3) provides an important metric. At this intercept point, the distortion due to the nonlinearity is severe as the third-order IMD has an equivalent output power to the fundamental signal. The IIP3 of the DFB laser is 29 dBm, which results in an OIP3 of 8.89 dBm, and the same outcomes can be observed with the theoretical simulation. However, such a high power is not an envisaged input power for the proposed system in this paper. From the estimation, the third-order IMD rises above the noise floor at the input power of 1 dBm. From Fig. 3, the theoretical and measured average SFDR of DFB laser is $\sim$57.83 dB, and the LTE requirement for SFDR metric is 55.9 dB [23]. The DFB laser used in our work could provide an additional SFDR of $\sim$1.93 dB. Additionally, it is desirable to maintain the input power close to 1 dBm for a minimum third-order IMD because the actual LTE signal is composed of OFDM modulation, which has a high peak-to-average ratio (PAPR). A lower dynamic range OFDM signal modulation will produce a higher nonlinearity from the clipping-induced distortion.

3. Optical Fiber Nonlinear Analysis

In the previous section, we have investigated the nonlinear response of the DFB laser based on direct modulation. The LTE signal propagation in the optical fiber could experience an additional nonlinearity with a high OLP. The nonlinear response of optical fiber propagation will emit additional

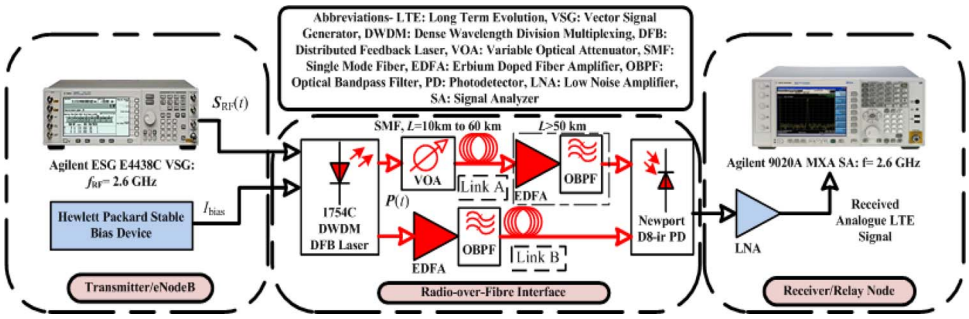

Fig. 4. Overall experimental setup of LTE-RoF system over 10–60-km transmission.

spurious signals. This section is dedicated to the investigation of the impact of nonlinear propagation on LTE signal from 10 to 60 km. In addition, we are also extending the investigation by exploring the deviation of the intermixing region with respect to the varying transmission distances. Since CD will accumulate with distance, it is important to determine if this accumulation would produce any additional nonlinear compensation and therefore shifting the intermixing region [24].

3.1. LTE-RoF Transmission Link

The experimental system shown in Fig. 4 is modeled in MATLAB. The important fundamental aspects of the system are as follows:

3.1.1. OFDM Modulation

At the transmitter, the signal in the baseband is composed of quaternary phase-shift keying (QPSK), 16-quadratic-amplitude modulation (QAM), and 64-QAM SCMs modulated signals. SCM modulated signals can be expressed as $\boldsymbol{X}(m)$ where $\{\boldsymbol{X}(m) : \mathrm{m} = 0, 1, \ldots, N-1\}$, $m = \sim$16 kHz is the subcarrier frequency, and $N = 2048$ is the number of subcarriers. $\boldsymbol{X}(m)$ are then modulated onto OFDM multicarrier modulation (MCM) $\boldsymbol{S}(n)$ [25]

$$\boldsymbol{S}(n) = \frac{1}{\sqrt{N}} \sum_{m=0}^{N-1} \boldsymbol{X}(m) e^{j2\pi mn/N} \tag{5}$$

where $\{n = 0, 1, \ldots\ldots, N-1\}$ is the time domain index. Cyclic prefix (CP) with the length of 512 (extended CP) is appended at the beginning of every OFDM symbol; however, it is important to specify that the normal CP length does not induce any degradation to the system [25]. The upconversion of $\boldsymbol{S}(n)$ with CP after a digital-to-analog converter can be described as

$$\boldsymbol{S}_{\mathrm{RF}}(t) = \mathrm{Re}\{\boldsymbol{S}(t) * \cos(\omega_{\mathrm{RF}} t)\} + \mathrm{Im}\{\boldsymbol{S}(t) * \sin(\omega_{\mathrm{RF}} t)\} \tag{6}$$

$$\omega_{\mathrm{RF}} = 2\pi f_{\mathrm{RF}} \tag{7}$$

where $\boldsymbol{S}_{\mathrm{RF}}(t)$ is the passband OFDM signal modulated at the frequency f_{RF} 2.6 GHz.

3.1.2. Direct Modulation and DFB

The electrical-to-optical conversion is carried out by directly modulating a DFB laser. Since the electrical signal is bipolar, therefore sufficient amount of I_{bias} is required to ensure the signal is all positive prior to the direct modulation

$$\boldsymbol{i}_{\mathrm{d}}(t) = I_{\mathrm{bias}}\{1 + \mu \boldsymbol{S}_{\mathrm{RF}}(t)\} \tag{8}$$

where $\boldsymbol{i}_{\mathrm{d}}(t)$ is the DFB driving current, and μ is the modulation index. While maintaining I_{bias} at 60 mA, $S_{\mathrm{RF}}(t)$ is linearly modulated. The theoretical modeling of a DFB laser is viable by adopting

the rate equations, namely, the rate of change of carrier density $d\boldsymbol{N}(t)/dt$ and the rate of change of photon density $d\boldsymbol{S}(t)/dt$, as given in (9) and (10). Finally, the directly modulated passband OOFDM can be obtained by solving the OLP equation $\boldsymbol{P}(t)$ that represents the signal at DFB laser output as given in (11) [8]

$$\frac{d\boldsymbol{N}(t)}{dt} = \frac{\boldsymbol{i}_{\mathrm{d}}(t)}{edwl} - \frac{N_{\boldsymbol{o}}+\boldsymbol{N}(t)}{\tau_{\mathrm{c}}} - B(N_{\boldsymbol{o}}+\boldsymbol{N}(t))^2 - C(N_{\boldsymbol{o}}+\boldsymbol{N}(t))^3 - G\frac{(N_{\boldsymbol{o}}+\boldsymbol{N}(t))-N_{\mathrm{t}}}{1+\varepsilon+(S_{\boldsymbol{o}}+\boldsymbol{S}(t))}(S_{\boldsymbol{o}}+\boldsymbol{S}(t)) \tag{9}$$

$$\frac{d\boldsymbol{S}(t)}{dt} = \Gamma G\frac{(N_{\boldsymbol{o}}+\boldsymbol{N}(t))-N_{\mathrm{t}}}{1+\varepsilon(S_{\boldsymbol{o}}+\boldsymbol{S}(t))}(S_{\boldsymbol{o}}+\boldsymbol{S}(t)) + \zeta B(N_{\boldsymbol{o}}+\boldsymbol{N}(t))^2 - \frac{(S_{\boldsymbol{o}}+\boldsymbol{S}(t))}{\tau_{\mathrm{p}}} \tag{10}$$

$$\boldsymbol{P}(t) = xw_{\mathrm{v}}w_{\mathrm{h}}hv\frac{(S_{\boldsymbol{o}}+\boldsymbol{S}(t))c}{2n_{\mathrm{g}}} \tag{11}$$

where e is the electronic charge; d is the thickness, w is the width, and l is the length of the laser cavity; N_o and S_o are the steady-state components; $\boldsymbol{N}(t)$ and $\boldsymbol{S}(t)$ are the carrier density and photon density, respectively; τ_{c} is the linear carrier recombination lifetime; B is the bimolecular carrier recombination coefficient; and C is the Auger carrier recombination coefficient. G represents the linear optical gain coefficient, N_{t} is the transparency carrier density, ε is the nonlinear gain coefficient, and Γ is the mode confinement factor. ζ represents the fraction of spontaneous emission, τ_{p} is the photon lifetime, χ is the coupling efficiency from the laser chip to the SMF, and w_{v} and w_{h} are the vertical and horizontal widths of the guided mode power distributions, respectively. h is the Planck's constant, v is the optical frequency, and c presents the speed of light in vacuum.

3.1.3. SMF

The transmission channel used in the RoF link is SMF. In principal, the SMF model that governs the properties of dispersive and nonlinear propagation can be expressed by the generalized nonlinear Schrödinger equation as [26]:

$$\begin{aligned}
\frac{\partial \boldsymbol{P}(L,t)}{\partial z} &= \left(\check{D}(L,t) + \check{N}(L,t) + \check{S}(L,t)\right) \times \boldsymbol{P}(L,t) \\
\check{D}(L,t) &= -\frac{j}{2}\beta_2\frac{\partial^2 \boldsymbol{P}(L,t)}{\partial T_o^2} - \frac{\alpha}{2} \\
\check{N}(L,t) &= j\frac{2\pi}{\lambda}n_2|\boldsymbol{P}(L,t)|^2 \\
\check{S}(L,t) &= -\frac{g_{\mathrm{B}}}{2A_{\mathrm{eff}}}|\boldsymbol{P}_{\mathrm{s}}(L,t)|^2\delta(\omega-\omega_{\mathrm{c}}) - \frac{\beta_{\mathrm{i}}}{2}
\end{aligned} \tag{12}$$

where $\boldsymbol{P}(L,t)$ is the OLP after propagating through L transmission span of SMF; $\check{D}(L,t)$ is the linear operator; $\check{N}(L,t)$ and $\check{S}(L,t)$ are the nonlinear operator for SPM and SBS, respectively; β_2 is the second-order dispersion coefficient; $T_o = t - z/v_{\mathrm{g}}$ is the time in a step that propagates at the group velocity v_{g}; α is the SMF attenuation coefficient; λ is the optical wavelength; n_2 is the nonlinear refractive index; g_{B} is the SBS gain; A_{eff} is the effective area; $\boldsymbol{P}_{\mathrm{s}}(L,t)$ is the reflected signal; and β_{i} is the spontaneous emission parameter.

3.1.4. Experimental Link

The overall experimental setup for LTE-RoF system is shown in Fig. 4. All system parameters are presented in Table 1. LTE signals generated for this experiment are $\boldsymbol{S}(n)$ with QPSK, 16-QAM and 64-QAM, and OFDM. At the complementary cumulative distribution function of 0.001%, PAPRs are $\sim$11.16 dB, $\sim$11.3 dB, and $\sim$11.67 dB for QPSK, 16-QAM, and 64-QAM, respectively. $\boldsymbol{S}_{\mathrm{RF}}(t)$ is generated at the real-time f_{RF} of 2.6 GHz via the vector signal generator (VSG).

The output of the VSG is directly applied to DFB laser to perform IM; the laser I_{bias} is fixed at 60 mA. Transmission links A and B are used for $\boldsymbol{P}(t)$ analysis with transmission spans in the range of 10–60 km. The link A is composed of a variable optical attenuator to investigate the

TABLE 1

System parameters

Parameters	Values
SCM modulations	QPSK, 16-QAM, 64-QAM
Number of subcarriers; subcarrier frequency; pilot type; frame length	2048; ~16 kHz; Block; 1 ms
Baseband multiplexing	OFDM
Cylic prefix size	¼ = 512
Bandwidth; Carrier frequencies	20 MHz; 2.6 GHz
RF power	2 dBm
DFB bias	60 mA
Optical power	-8 dBm to 10 dBm
RIN	-149.6 dB/Hz
SMF length	10 km to 60 km
EDFA gain, noise figure	2 dB to 6 dB, 3.5 dB
PD responsivity	0.42
LNA- gain, noise figure	18 dB, 2.5 dB

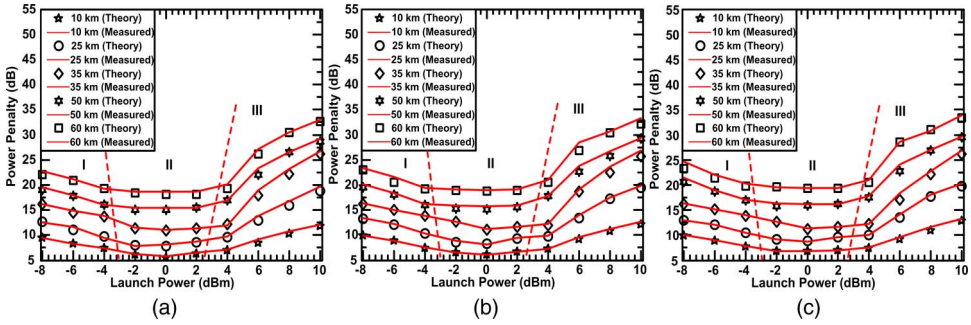

Fig. 5. OLP against power penalty analysis of (a) QPSK, (b) 16-QAM, and (c) 64-QAM with transmission span of 10–60 km.

lower $\boldsymbol{P}(t)$. An erbium-doped fiber amplifier (EDFA) and an optical bandpass filter (OBPF) are utilized for link A for a transmission span L of more than 50 km to compensate for the fiber loss as the PD responsivity is low, in addition to the low noise amplifier (LNA) used following the DD of the optical signal. The link B consists of an EDFA and an OBPF for higher $\boldsymbol{P}(t)$ analysis. Signals propagating through all links are detected via the DD scheme.

In a conventional system, this detected signal will be forwarded to UE via the RF wireless antenna. In this paper, the signal is analyzed with the Agilent 9020A MXA SA to examine the signal quality. The discussion on the OLP analysis and linear and nonlinear thresholds will be carried out in the next section with considering the power penalty and the error vector magnitude (EVM).

3.2. OLP Analysis

The distortion induced by optical fiber propagation from CD, PFC with SPM and SBS can be minimized by optimizing $\boldsymbol{P}(t)$. The optimal control of $\boldsymbol{P}(t)$ would compensate CD and PFC with higher SPM and SBS effect, vice versa if the motive of the system design is to compensate the system nonlinearity. This approach is cost effective since there is no additional optical equalizing device required in the system design. The optical fiber propagation can be categorized into three distinctive optical power transmission regions, as shown in Fig. 5, namely, I) linear region—PFC- and CD-induced distortion, II) intermixing region—reduced distortion achieved by the interaction between CD and PFC with SPM and SBS, and finally, III) nonlinear region—nonlinearity-based distortion from SPM and SBS effect. One of the important aspects of this section is to investigate

whether varying the transmission spans would cause deviation in the location of the minimum power penalty range of region II.

Fig. 5(a)–(c) depicts the power penalty of QPSK, 16-QAM, and 64-QAM systems, compared with the back-to-back system, respectively, for transmission spans of 10, 25, 35, 50, and 60 km. $\boldsymbol{P}(t)$ is varied in the range of -8 dBm to 10 dBm to investigate optical power transmission regions. In region I of QPSK, 16-QAM and 64-QAM systems, for the range of $\boldsymbol{P}(t) < -3$ dBm, the power penalty increases with decreasing $\boldsymbol{P}(t)$ for all transmission distances. Fundamentally, as $\boldsymbol{P}(t)$ decreases, the signal-to-noise ratio (SNR) decreases, thus illustrating the linear relationship with respect to the impairment occurred in region I. The discussion on results is focused on the shortest transmission span of 10 km and farthest transmission span of 60 km as all curves exhibit a similar pattern. At the lowest $\boldsymbol{P}(t)$ of -8 dBm for 10-km transmission span, QPSK, 16-QAM, and 64-QAM systems experience power penalties of $\sim$9.48 dB, $\sim$9.97 dB, and $\sim$9.98 dB, respectively, whereas at 60 km, the power penalties are $\sim$22.8 dB, $\sim$23.4 dB, and $\sim$24.6 dB, respectively. It is clear from Fig. 5 that the power penalties of the theoretical system match the experimentally measured values, thus validating the theoretical system design.

In region III of Fig. 5(a)–(c) for the range of $\boldsymbol{P}(t) > 4$ dBm, QPSK, 16-QAM, and 64-QAM system power penalties increase with $\boldsymbol{P}(t)$, for all the aforementioned transmission spans, respectively. This phenomenon indicates that SNR deteriorates despite increasing $\boldsymbol{P}(t)$, which is mainly due to the nonlinear phase distortion and the back-reflection. At $\boldsymbol{P}(t)$ of 10 dBm for 10-km transmission span, QPSK, 16-QAM, and 64-QAM system power penalties are $\sim$12.1 dB, $\sim$12.7 dB, and $\sim$13.2 dB, respectively, whereas at 60 km, the power penalties are $\sim$33 dB, $\sim$33.33 dB, and $\sim$33.9 dB, respectively. The power penalties in region III are higher than those in region I because the nonlinear distortion will actuate out-of-band emission and increase the noise floor level. In other words, the actual power of $\boldsymbol{P}(t)$ is transferred and modulated to the back-reflected Stokes' signal, where the reflected signal will arrive at PD as a random time-varying Gaussian noise with a broad spectral characteristic centered on the received signal and directly increases the noise floor [27], [28]. The power transfer of $\boldsymbol{P}(t)$ and the rise in the noise floor are major factors of the high power penalty. The nonlinear propagation will also induce additional in-band distortion, which will be analyzed and discussed with the aid of EVM measurement later in this section.

The optimum power penalty is achieved in region II (intermixing region), from -2 dBm to 2 dBm, as shown in Fig. 5. It can be observed from Fig. 5(a)–(c) for QPSK, 16-QAM, and 64-QAM systems, respectively, that as the transmission link increases, the intermixing region remains within this range. Linear distortions are known to accumulate with the distances [24], but our investigation fundamentally shows that both linear and nonlinear impairments increase proportionally with the transmission span. In region II, average power penalties for QPSK, 16-QAM, and 64-QAM systems at the transmission span of 10 km are $\sim$6.17 dB, $\sim$6.48 dB, and $\sim$6.88 dB, respectively, whereas at 60 km, the resultant power penalties are $\sim$18.64 dB, $\sim$19.08 dB, and $\sim$19.47 dB, respectively. Considering the 60-km transmission span, the improvements observed in the intermixing region (region II) for the QPSK system with respect to region I ($\boldsymbol{P}(t) = -4$ dBm) and region III ($\boldsymbol{P}(t) = 4$ dBm) are $\sim$0.66 dB and $\sim$1.46 dB, respectively. Likewise, for the 16-QAM system, comparing with region I ($\boldsymbol{P}(t) = -4$ dBm) and region III ($\boldsymbol{P}(t) = 4$ dBm), the improvements are $\sim$0.42 dB and $\sim$1.88 dB, respectively. The improvements associated with the 64-QAM system with respect to region I ($\boldsymbol{P}(t) = -4$ dBm) and region III ($\boldsymbol{P}(t) = 4$ dBm) are $\sim$0.83 dB and $\sim$1.53 dBm, respectively.

The impact of distortion induced within the finite bandwidth of the signal can be characterized by the EVM. The proposed system is designed to achieve EVM lower than the required 8% specified by 3GPP for LTE [29]. Fig. 6(a)–(c) depicts the EVM of QPSK, 16-QAM, and 64-QAM systems, respectively. Graphs are categorized into three distinctive regions similar to the optical power transmission regions. The observed EVMs for QPSK, 16-QAM, and 64-QAM systems at $\boldsymbol{P}(t)$ of -8 dBm (region I) for 10-km transmission span are $\sim$1.402%, $\sim$1.43%, and $\sim$1.51%, respectively, whereas at 60 km, the EVMs are $\sim$7.42%, $\sim$7.73%, and $\sim$7.82%, respectively. It is shown in Fig. 6(a)–(c) that the linearly distorted DD-OOFDM signals in this region I are below the specified EVM. In region III, at $\boldsymbol{P}(t)$ of 10 dBm, QPSK, 16-QAM, and 64-QAM systems have achieved EVMs

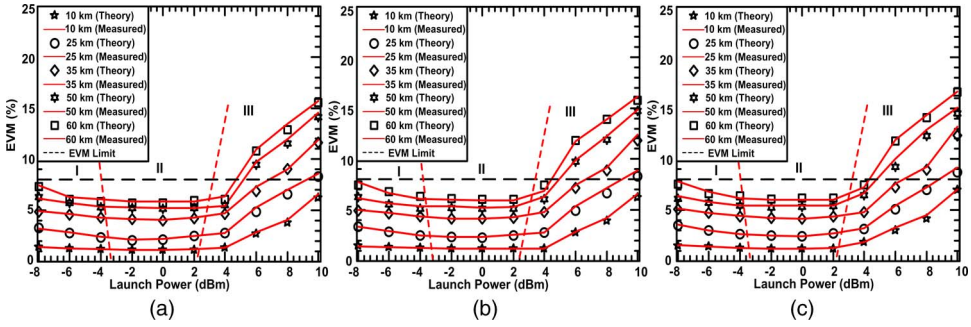

Fig. 6. OLP against EVM analysis of (a) QPSK, (b) 16-QAM, and (c) 64-QAM with transmission span of 10–60 km.

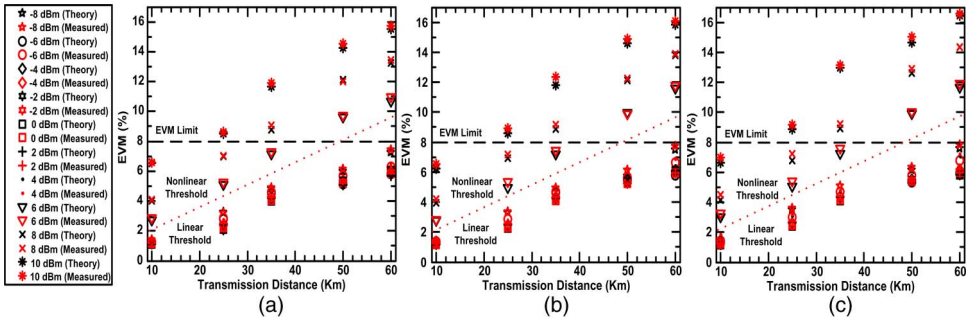

Fig. 7. Transmission distance against EVM analysis of (a) QPSK, (b) 16-QAM, and (c) 64-QAM.

of ∼6.57%, ∼6.55%, and ∼6.97%, respectively, for 10-km transmission span, whereas at 60 km, the resultant EVMs are ∼15.732%, ∼16.1%, and ∼16.6%, respectively. It is clearly shown in Fig. 6 that only the 10-km transmission span has achieved less than 8% EVM at 10 dBm $\boldsymbol{P}(t)$ (region III). This is due to the nonlinear propagation that induces in-band distortion, which will lead to the severe intercarrier interference for longer spans.

The intermixing region (region II) provides the optimum EVM. In Fig. 6(a), QPSK, 16-QAM, and 64-QAM systems at 10-km transmission span have achieved average EVMs of ∼1.144%, ∼1.2%, and ∼1.21%, respectively, whereas at 60 km, average EVMs are ∼5.86%, ∼5.96%, and ∼6.01%, respectively. The aforementioned EVMs for 60 km are the best achievable case for LTE signal transmission over RoF without any optical equalization devices. In terms of the deviation in the optimum region, the optimum $\boldsymbol{P}(t)$ range is consistent throughout the 10–60-km transmission range, which proves that the linear and nonlinear distortion increases proportionally within transmission distance.

3.3. Direct Modulation Nonlinear Threshold

It is important to understand the evolving nature of linear and nonlinear distortions with respect to the transmission distance. Fig. 7(a)–(c) shows QPSK, 16-QAM, and 64-QAM propagation characteristics for a range of $\boldsymbol{P}(t)$ with respect to EVM. It is clear that QPSK, 16-QAM, and 64-QAM systems experience a pronounced nonlinear distortion for $\boldsymbol{P}(t) > 6$ dBm. As a result, $\boldsymbol{P}(t)$ at 6 dBm is the "direct modulation nonlinear threshold" where, for $\boldsymbol{P}(t)$ above this threshold, the signal will experience severe EVM degradation. Graphs also indicate that, irrespective of the propagation state, the distortion linearly increases with transmission distance.

4. Conclusion

In this paper, we have proposed and demonstrated the SFDR analysis of direct modulation based on DFB laser and the full LTE-RoF system transmission span ranging from 10 to 60 km. We have

shown theoretically and experimentally that direct modulation provides 1.93-dB additional SFDR for the signal modulation; therefore, it is both cost effective and modulation efficient. In LTE-RoF system, the paper presented practical optical power transmission regions that conform to the earlier theoretical investigation. While transmitting in region I (CD- and PFC-induced distortions), it is still possible to achieve below the 3GPP EVM margin of less than 8% for 10–60-km transmission spans. However, signal propagating in region III (SPM- and SBS-induced distortions) experiences severe distortion, where only 10-km transmission distance could attain the EVM limit of less than 8% across the whole range of $\boldsymbol{P}(t)$. At the intermixing region (region II), in comparison with region I, the measurement showed power gains of $\sim$0.66 dB, $\sim$0.42 dB, and $\sim$0.83 dB for QPSK, 16-QAM, and 64-QAM, respectively, for 60-km transmission span. The power gains observed in region II with respect to region III are $\sim$1.46 dB, $\sim$1.88 dB, and $\sim$1.53 dB for QPSK, 16-QAM, and 64-QAM, respectively, at 60-km transmission span. The study also revealed that, irrespective of transmission span, region II does not deviate and remains within the same range. Finally, we presented the direct modulation nonlinear threshold for LTE-RoF system. The investigation showed that the system experiences severe nonlinear distortion for $\boldsymbol{P}(t) < 6$ dBm, while both linear and nonlinear distortions increase linearly with the transmission distance.

References

[1] T. Wirth, V. Venkatkumar, T. Haustein, E. Schulz, and R. Halfmann, "LTE-advanced relaying for outdoor range extension," in *Proc. IEEE 70th VTC*, 2009, pp. 1–4.

[2] M. S. David, F. M. Jose, C. P. Jorge, C. Daniel, G. Salvador, and C. Narcis, "On the way towards fourth-generation mobile: 3GPP LTE and LTE-advanced," *EURASIP J. Wireless Commun. Netw.*, vol. 2009, pp. 354089-1–354089-10, Mar. 2009.

[3] D. Soldani and S. Dixit, "Wireless relays for broadband access [radio communications series]," *IEEE Commun. Mag.*, vol. 46, no. 3, pp. 58–66, Mar. 2008.

[4] K. Dimou, W. Min, Y. Yu, M. Kazmi, A. Larmo, J. Pettersson, W. Muller, and Y. Timner, "Handover within 3GPP LTE: Design principles and performance," in *Proc. IEEE 70th VTC*, 2009, pp. 1–4.

[5] S. W. Peters, A. Y. Panah, K. T. Truong, and J. R. W. Heath, "Relay Architectures for 3GPP LTE-Advanced," *EURASIP J. Wireless Commun. Netw.*, vol. 2009, pp. 618787-1–618787-14, 2009.

[6] A. Nagate, K. Hoshino, M. Mikami, and T. Fujii, "A field trial of multi-cell cooperative transmission over LTE system," in *Proc. IEEE ICC*, 2011, pp. 1–5.

[7] D. Turner, "Evolution to LTE and the surrounding challenges for in-building coverage," in *Proc. Zinwave*, 2011, pp. 1–12.

[8] T. Kanesan, W. P. Ng, Z. Ghassemlooy, and J. Perez, "Optimization of optical modulator for LTE RoF in nonlinear fiber propagation," *IEEE Photon. Technol. Lett.*, vol. 24, no. 7, pp. 617–619, Apr. 2012.

[9] O. Tipmongkolsilp, S. Zaghloul, and A. Jukan, "The evolution of cellular backhaul technologies: Current issues and future trends," *IEEE Commun. Surveys Tuts.*, vol. 13, no. 1, pp. 97–113, First Quarter, 2011.

[10] D. Wake, A. Nkansah, N. J. Gomes, G. de Valicourt, R. Brenot, M. Violas, L. Zhansheng, F. Ferreira, and S. Pato, "A comparison of radio over fiber link types for the support of wideband radio channels," *J. Lightw. Technol.*, vol. 28, no. 16, pp. 2416–2422, Aug. 2010.

[11] F. S. Yang, M. E. Marhic, and L. G. Kazovsky, "Nonlinear crosstalk and two countermeasures in SCM–WDM optical communication systems," *J. Lightw. Technol.*, vol. 18, no. 4, pp. 512–520, Apr. 2000.

[12] F. Ramos, J. Marti, V. Polo, and J. M. Fuster, "On the use of fiber-induced self-phase modulation to reduce chromatic dispersion effects in microwave/millimeter-wave optical systems," *IEEE Photon. Technol. Lett.*, vol. 10, no. 10, pp. 1473–1475, Oct. 1998.

[13] H. Bao and W. Shieh, "Transmission simulation of coherent optical OFDM signals in WDM systems," *Opt. Exp.*, vol. 15, no. 8, pp. 4410–4418, Apr. 2007.

[14] S. Ju Bin and A. H. M. R. Islam, "Distortion of OFDM signals on radio-over-fiber links integrated with an RF amplifier and active/passive electroabsorption modulators," *J. Lightw. Technol.*, vol. 26, no. 5, pp. 467–477, Mar. 2008.

[15] V. Ali, J. Leibrich, and W. Rosenkranz, "Impact of nonlinearities on optical OFDM with direct detection," in *Proc. 33rd ECOC*, 2007, pp. 1–2.

[16] K. Kyoungsoo, L. Jaehoon, and J. Jichai, "Performance limitations of subcarrier multiplexed WDM signal transmissions using QAM modulation," *J. Lightw. Technol.*, vol. 27, no. 18, pp. 4105–4111, Sep. 2009.

[17] M. A. Jarajreh, Z. Ghassemlooy, and W. P. Ng, "Improving the chromatic dispersion tolerance in long-haul fibre links using the coherent optical orthogonal frequency division multiplexing," *IET Microw., Antennas Propag.*, vol. 4, no. 5, pp. 651–658, May 2010.

[18] M. A. Jarajreh, J. L. Wei, J. M. Tang, Z. Ghassemlooy, and W. P. Ng, "Effect of number of sub-carriers, cyclic prefix and analogue to digital converter parameters on coherent optical orthogonal frequency division multiplexing modem's transmission performance," *IET Commun.*, vol. 4, no. 2, pp. 213–222, Jan. 2010.

[19] K.-P. Ho, *Phase-Modulated Optical Communications System*. New York: Springer-Verlag, 2005.

[20] G. S. D. Gordon, M. J. Crisp, R. V. Penty, and I. H. White, "High-order distortion in directly modulated semiconductor lasers in high-loss analog optical links with large RF dynamic range," *J. Lightw. Technol.*, vol. 29, no. 23, pp. 3577–3586, Dec. 2011.

[21] M. N. Draa, J. Ren, D. C. Scott, W. S. C. Chang, and P. K. L. Yu, "Three laser two-tone setup for measurement of photodiode intercept points," *Opt. Exp.*, vol. 16, no. 16, pp. 12108–12113, Aug. 2008.
[22] F. Vacondio, M. Mirshafiei, J. Basak, L. Ansheng, L. Ling, M. Paniccia, and L. A. Rusch, "A silicon modulator enabling RF over fiber for 802.11 OFDM signals," *IEEE J. Sel. Topics Quantum Electron.*, vol. 16, no. 1, pp. 141–148, Jan./Feb. 2010.
[23] S. Sesia, M. Baker, and I. Toufik, *LTE, The UMTS Long Term Evolution: From Theory to Practice*. New York: Wiley, 2009.
[24] K. Forozesh, S. L. Jansen, S. Randel, I. Morita, and H. Tanaka, "The influence of the dispersion map in coherent optical OFDM transmission systems," in *Proc. Dig. IEEE/LEOS Summer Topical Meetings*, 2008, pp. 135–136.
[25] 3GPP, Evolved Universal Terrestrial Radio Access (E-UTRA); Physical channels and modulation (3GPP TS 36.211 V10.4.0 Rel-10), ETSI, Sophia Antipolis, France, 2011.
[26] A. Djupsjobacka, C. Jacobsen, and B. Tromborg, "Dynamic stimulated Brillouin scattering analysis," *J. Lightw. Technol.*, vol. 18, no. 3, pp. 416–424, Mar. 2000.
[27] Y. Aoki, K. Tajima, and I. Mito, "Input power limits of single-mode optical fibers due to stimulated Brillouin scattering in optical communication systems," *J. Lightw. Technol.*, vol. 6, no. 5, pp. 710–719, May 1988.
[28] A. Yariv, H. Blauvelt, D. Huff, and H. Zarem, "An experimental and theoretical study of the suppression of interferometric noise and distortion in AM optical links by phase dither," *J. Lightw. Technol.*, vol. 15, no. 3, pp. 437–443, Mar. 1997.
[29] 3GPP, EVM for LTE Repeater (3GPP TSG-RAN4 Meeting #52, TS 36.143, Rel-8), Andrew Wireless Systems, Powerwave Technologies, Shenzhen, China, 2009.